IOP PUBLISHING PHYSIOLOGICAL MEASUREMENT

Physiol. Meas. **28** (2007) 515–529 doi:10.1088/0967-3334/28/5/006

Tripolar Laplacian electrocardiogram and moment of activation isochronal mapping

W Besio and T Chen

Department of Biomedical Engineering, Louisiana Tech University, 711 South Vienna St., Ruston, LA, USA

E-mail: walterb@latech.edu

Received 8 November 2006, accepted for publication 20 March 2007
Published 20 April 2007
Online at stacks.iop.org/PM/28/515

Abstract

The electrocardiogram (ECG) provides useful global temporal assessment of the cardiac activity, but has limited spatial capabilities. The Laplacian electrocardiogram (LECG), an improvement over the ECG, provides high spatiotemporal distributed information about cardiac electrical activation. We designed and developed LECG tripolar concentric ring electrode active sensors based on the finite element algorithm 'nine-point method' (NPM). The active sensors were used in an array of 6 by 12 (72) locations to record bipolar and tripolar LECG from the body surface over the anterolateral chest. Compared to bipolar LECG, tripolar LECG showed significantly higher spatial selectivity which may be helpful in inferring information about cardiac activations detected on the body surface. In this study the moment of activation (MOA), an indicator of a depolarization wave passing below the active sensors, was used to surmise possible timing information of the cardiac electrical activation below the active sensors' recording sites. The MOA on the body surface was used to generate isochronal maps that may some day be used by clinicians in diagnosing arrhythmias and assessing the efficacy of therapies.

Keywords: Laplacian electrocardiogram (LECG), tripolar concentric ring electrode (TCE), nine-point method (NPM), spatial selectivity, active sensor

(Some figures in this article are in colour only in the electronic version)

1. Introduction

Non-invasive evaluation of cardiac electrical activation is currently of interest in clinical applications for its effectiveness and timeliness. Body surface Laplacian mapping (BSLM) has been shown to be an alternative to BSPM with a better spatial resolution and enhanced

capability of localization by using the estimated Laplacian of body surface potentials to create maps (Oostendorp and Oosterom 1996, He and Cohen 1991, 1992, 1995, He and Wu 1999, Umetani *et al* 1998, Wu *et al* 1998, 1999, He 1998, Ono *et al* 1997, Lian *et al* 2002a, 2002b, Li *et al* 2002, 2003, He *et al* 2002, Besio and Tarjan 2002a, 2002b, Besio *et al* 2001, Besio 2001). The Laplacian is the second spatial derivative of the potentials on the body surface which reduces the smoothing effect of the torso volume conduction and provides more details in localizing and differentiating multiple concurrent dipole sources (He and Cohen 1992). The surface Laplacian can also be interpreted as an equivalent current density (He and Cohen 1992, 1995). Several studies (Umetani *et al* 1998, He and Wu 1999, Wu *et al* 1999, He *et al* 2002, Lian *et al* 2002b, Li *et al* 2003) utilized large numbers of unipolar electrodes placed on the chest surface to measure the body surface potentials, and from that data the Laplacian electrocardiogram (LECG) was derived by using a five-point finite difference algorithm (FPM) or a spline surface Laplacian estimator.

Fattorusso and Tilmant (1949) were the first to use bipolar concentric ring electrodes in cardiology. He and Cohen (1991, 1992, 1995) developed a bipolar concentric electrode to directly measure the body surface LECG and demonstrated that the LECG has a better spatial resolution in resolving and imaging spatially distributed cardiac electrical activation than body surface potentials.

Lu and Tarjan (1999) developed an active LECG sensor with a tripolar concentric ring electrode (TCE) where the outer ring and the center disc were electrically shorted. This TCE with the outer ring and the center disc shorted is referred to here as a quasi-bipolar sensor (QBS). Besio *et al* (2001), Besio (2001), Besio and Tarjan (2002a, 2002b) demonstrated the efficacy of using this QBS for detecting atrial activation patterns by recording from 35 locations on the chest surface. Based on the nine-point method (NPM) (Besio *et al* 2006), a new active Laplacian TCE sensor was designed without the outer ring and the center disc electrically shorted.

For this study we used the new active Laplacian TCE sensor (Besio and Chen 2006) to acquire signals. The averaged cardiac activation cycle of the LECG on the body surface, BSLM which shows the Laplacian potential distribution at the time instant of the Lead II ECG R-wave peak, and Laplacian moment of activation (MOA) isochronal mapping (Besio *et al* 2001, Besio 2001, Besio and Tarjan 2002a, 2002b) were performed. The BSLM was used to relate the multiple earlier activation areas of the MOA map with respect to the underlying cardiac electrical activations.

2. Methods

2.1. Design of an active LECG TCE sensor and signal pre-processing

In the present study the active sensor and signal pre-processing were developed using the TCE for acquiring body surface LECG. Equation (1) (Besio *et al* 2006) shows the new algorithm for approximating the surface tripolar Laplacian with the TCE:

$$\Delta V \cong \frac{1}{3r^2}[16 \times (V_{\mathrm{mr}} - V_c) - 1 \times (V_{\mathrm{or}} - V_c)] \tag{1}$$

where V_{or}, V_{mr} and V_c denote the average potentials on the TCE elements which include outer, middle and center electrode elements, respectively (figure 1(A)), and r is the inter-element distance. To be compatible with the LECG definition (He and Cohen 1995, He and Wu 1999),

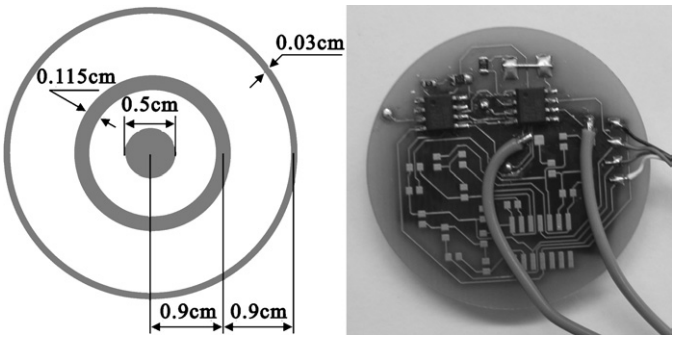

Figure 1. The new active LECG TCE sensor. (A) Schematic of the electrodes. (B) The circuit side of the sensor. Two flexible shielded cables were used to connect the signals from the instrumentation amplifiers to a Grass amplifier system (Grass Telefactor, 15LT, W Warwick, RI, USA).

the negative of the surface Laplacian was used in this study as shown in (2):

$$L_{\text{tripolar}} = -\Delta V \cong -\frac{1}{3r^2}[16 \times (V_{\text{mr}} - V_c) - 1 \times (V_{\text{or}} - V_c)]$$
$$= \frac{1}{3r^2}[1 \times (V_{\text{or}} - V_c) - 16 \times (V_{\text{mr}} - V_c)]. \quad (2)$$

On the new active LECG TCE sensor, two ultra-high input impedance instrumentation amplifiers (IA) were used for the first stage amplification of signals from the TCE. These two IAs performed the two differences between each concentric ring and the center disc. The gains of the first stage amplification were both set to 10. The output signals from these two IAs were connected to a Grass amplifier system (1–500 Hz, gain 2000; total gain 20 000). For the tripolar LECG the signals from the Grass amplifier were digitized (described later) and then pre-processed based on equation (2).

The two IAs are implemented on one side of a printed circuit board (PCB). Figure 1(B) depicts the circuit side of this new design. On the other side of the sensor board are the TCE which are gold-plated copper for good electrical conductivity. The dimensions of the TCE are shown in figure 1(A). The potential differences between each concentric ring and the center disc are recorded simultaneously to acquire LECG.

To determine whether the tripolar LECG provides better spatial selectivity than the bipolar LECG (He and Cohen 1992, Besio *et al* 2006), the tripolar and bipolar LECG were recorded simultaneously and compared in this study. Equation (3) shows the algorithm for approximating the bipolar LECG (He and Cohen 1992, Besio *et al* 2006):

$$L_{\text{bipolar}} = -\Delta V \cong -\frac{4}{(2r)^2}(V_{\text{or}} - V_c) = \frac{1}{r^2}(V_c - V_{\text{or}}). \quad (3)$$

In the signal pre-processing the bipolar LECG was obtained as the negative value of the outer ring to disc potential difference (He and Cohen 1992, Besio *et al* 2006). Thus the tripolar and bipolar LECGs were recorded with the same conditions.

2.2. Data acquisition system

Six active LECG TCE sensors and one Lead II ECG sensor, which served as a time reference, were used to record the cardiac body surface data. Thirteen channels of data, two for each active LECG TCE sensor and one for the Lead II ECG sensor, were recorded simultaneously

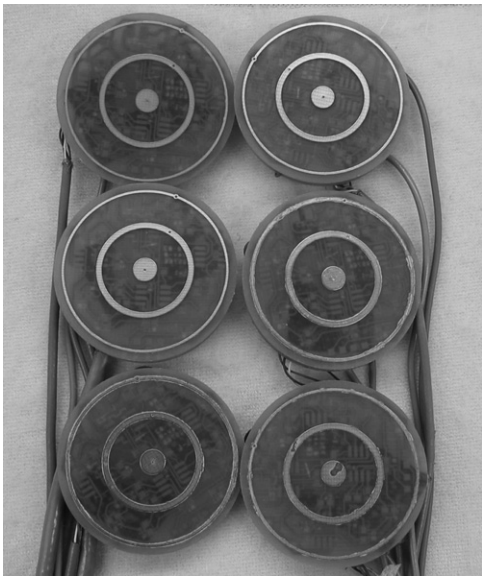

Figure 2. The electrode side of six active LECG TCE sensors configured in a 3 row by 2 column matrix and attached to the inside of a wide elastic strap. Three gold-plated electrode elements on each sensor's back side make contact with the body surface.

(16 bit, 2 kHz, 30 s, Dataq Instruments DI-720 Series, Akron, OH, USA) to a battery-powered laptop. The active LECG TCE sensors were also battery-powered.

2.3. LECG acquisition from human subjects

All signal acquisition was performed in accordance with the Louisiana Tech University IRB approved protocol. Signals were recorded from six healthy male subjects of 20–25 years. The six active LECG TCE sensors were attached inside a wide elastic strap as shown in figure 2. The strap was wrapped around the body to hold the electrodes in place. A thin coat of Ten20 electrode paste (DO Weaver and Co, Aurora, CO, USA) was spread uniformly on the electrodes.

While recording, the subjects lay in a supine position and were asked to relax and remain stationary to avoid the influence of fluctuations of the heart position on the body surface ECG and LECG (Macleod *et al* 2000). The actual recordings were repeated with the active LECG TCE sensor array moved to each of the preplanned locations with 1.2 cm horizontal spatial sampling resolution on the chest. In the recording sensor array, the distance between two adjacent electrodes' center discs was 3.6 cm (inter-electrode spacing). The red dots/square markers in figure 3 show the first six locations recorded. Then the array was translated 1.2 cm horizontally to the green dots/open circle markers and again to the blue dots/triangle markers for a total of 18 recording sites. Eighteen more locations (3 row by 6 column) were recorded by moving the sensor array 4.8 cm horizontally to cover the next recording surface with two more translations. Then after recording the surface above the nipple line, the sensor array was moved downward to cover the surface under the nipple line with the same process repeated. The total 6 row by 12 column matrix body surface cardiac LECG signals were recorded for each subject from 72 locations as shown in figure 3.

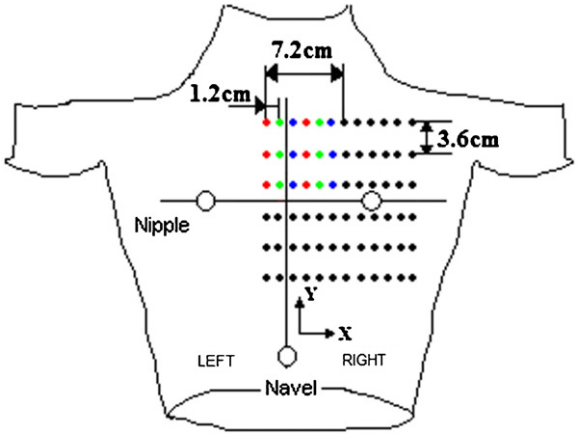

Figure 3. The 6 row by 12 column matrix of recording sites over the anterolateral chest, a frontal view. Each dot/marker represents a recording site. Horizontal and vertical distances between the two recording sites are 1.2 and 3.6 cm respectively. The nipple line and sternal midline are references for the recording sites and are represented with dashed lines. The intersection of these two lines was the origin. Right and left from the reader's perspective are used to designate two sides of the sternal midline.

2.4. LECG post-processing

The right hip was used as the recording reference for each subject. The LECG data were baseline-adjusted for drift before it was Weiner filtered (He and Wu 1999, He 1998). In post-processing, each LECG signal was windowed and synchronized relative to the simultaneously recorded Lead II ECG R-wave peak after performing QRS detection (Besio and Kota 2004). A 1600-point window digital Weiner filter was applied to cover one 800 ms cardiac cycle. Then the Weiner filtered LECG were ensemble averaged, based on the 800 ms window.

2.5. LECG MOA algorithm

The MOA is defined as 'the instant the dipole that represents the depolarization wavefront crosses the vector normal to the active sensor's surface' (Besio *et al* 2001). There is a delay for the depolarization wavefront to propagate over the body surface. The MOA is determined by calculating the time when the dipoles' activation wavefront may be directly below the sensor. An array of active LECG TCE sensors provides spatial information about the propagation delays on the body surface. Cross-correlation for pattern matching between the LECG and Lead II ECG was used to find the best fit. The time offset between these two similar waves was designated as the MOA with the units in (ms). A new algorithm for detecting MOA (Besio and Kota 2004) was automated and achieved greater than 99% efficiency on simulated signals with noise. The MOA could be zero, which means the LECG wave happens at the same time as the Lead II ECG R-wave peak. A positive MOA means the LECG wave happens later than the Lead II ECG R-wave peak, and a negative value means the LECG wave happens earlier than the Lead II ECG R-wave peak.

2.6. Comparison of spatial selectivity

To compare the spatial selectivity, we used the SSy. The SSy is calculated as the average of the ratios of the peak-to-peak values of the LECG at one recording site among its four neighboring

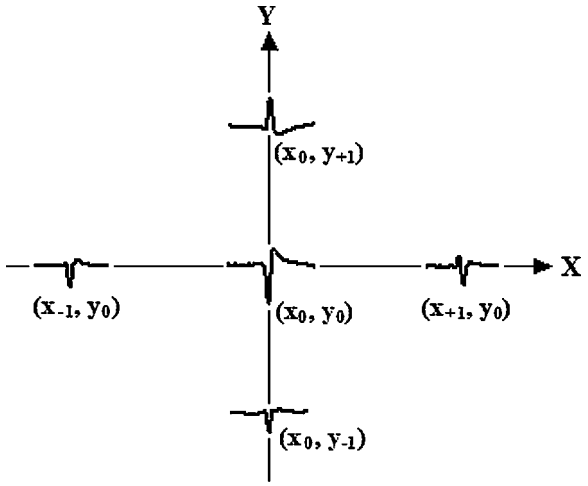

Figure 4. Illustration of the calculation of the SSy.

recording sites (twelve o'clock, three o'clock, six o'clock and nine o'clock around the non-marginal recording site). For consistency between subjects we calculated the SSy on an area where the magnitude of the central signal was greater than its four immediate neighbors. For example $\mathrm{SSy}(x_0, y_0)$ was calculated as follows:

$$\mathrm{SSy}(x_0, y_0) = \left(\frac{P(x_0, y_0)}{P(x_{-1}, y_0)} + \frac{P(x_0, y_0)}{P(x_{+1}, y_0)} + \frac{P(x_0, y_0)}{P(x_0, y_{-1})} + \frac{P(x_0, y_0)}{P(x_0, y_{+1})} \right) \Big/ 4 \tag{4}$$

where x_0 and y_0 are the LECG coordinates in x and y directions, respectively, shown in figure 3. $P(x_0, y_0)$, $P(x_{-1}, y_0)$, $P(x_{+1}, y_0)$, $P(x_0, y_{-1})$ and $P(x_0, y_{+1})$ denote the peak-to-peak values of LECG at location (x_0, y_0) and its four adjacent LECG, respectively (figure 4). When calculating the SSy at (x_0, y_0) using equation (4), a large SSy means that there is a stronger signal at (x_0, y_0) compared to its neighboring signals. Higher SSy may improve the ability of differentiating the central signal from its neighboring signals, increasing the spatial selectivity.

3. Results

3.1. Tripolar LECG waves

We were able to record signals from healthy males with the new active LECG TCE sensors. In figure 5, panels A, B and C show three examples of processed tripolar LECG acquired at different recording locations from a subject (no 4), which were the typical waveforms in all six subjects. Panel D is the relative Lead II ECG. The LECG in panel A is a monophasic negative wave. Similarly the LECG in panel B is a monophasic positive wave. The LECG in panel C is a biphasic (doublet) wave that has a strong positive/negative pulse followed by a strong negative/positive pulse.

In figure 5, the durations of the QRS waves are indicated between two dashed lines in each panel. For consistency, the first zero crossing before and after the peak determined the start and end of each QRS wave. It can be seen that the duration of the LECG QRS waves was shorter than that of the Lead II ECG. For all six subjects, the ranges of the duration of the LECG QRS waves were: monophasic negative 24–43 ms (35 ± 6.90 ms), monophasic positive 22–46 ms (36.17 ± 8.26 ms) and biphasic 47–65 ms (57 ± 6.48 ms). For the Lead II ECG QRS waves the range of duration was between 97 ms and 117 ms (108.67 ± 6.83 ms).

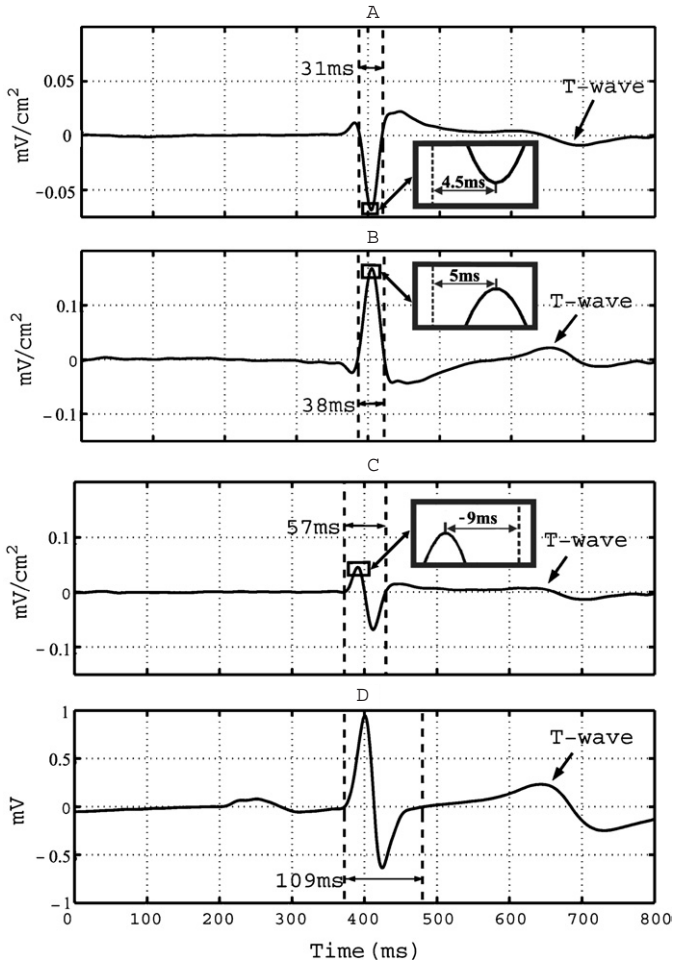

Figure 5. Tripolar LECG: panel A (monophasic negative), panel B (monophasic positive) and panel C (biphasic/doublet); panel D is the relative Lead II ECG recorded simultaneously. The abscissa designates the time in 100 ms increments. The ordinate designates the magnitude of the waveform with the units in (mV cm^{-2}) for LECG and (mV) for Lead II ECG. T-waves are marked in the figure.

Panels A, B and C reflect that the T-wave which represents ventricular repolarization can be seen clearly with different polarities in the LECG.

In figure 5 the MOA are also shown for the LECG in panels A, B and C. As a reference for calculating MOA, the R-wave peak of Lead II ECG was set to the position corresponding to 400 ms. Then the MOA was designated as the time difference between the position of the highest correlated LECG wave and 400 ms. In figure 5, the MOA was 4.5 ms, 5.0 ms and −9.0 ms for LECG in panels A, B and C, respectively.

3.2. Comparison of the tripolar and bipolar LECG

Both tripolar and bipolar LECG were recorded simultaneously. Figure 6 shows one averaged cardiac activation cycle of the LECG recorded from the anterolateral chest surface of the same subject's (no 4) signals. Panels A and B represent tripolar and bipolar LECG respectively. The

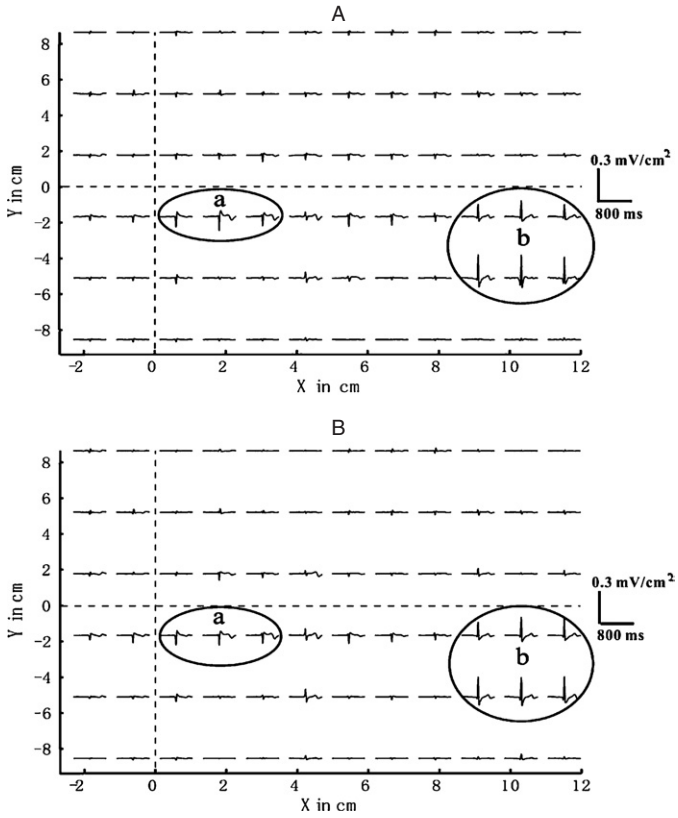

Figure 6. One averaged cardiac activation cycle of LECG in a 6 row by 12 column topology recorded from the anterolateral chest of subject no 4. Panels A and B represent tripolar and bipolar LECG, respectively. The abscissa and ordinate designate the recording location over the chest measured in (cm). The two dashed lines correspond to the nipple line and sternal midline.

LECG waveforms are shown in a 6 row by 12 column topology with respect to the recording sites of figure 3.

The LECG presented in panels A, B and C of figure 5 are represented in figure 6 at locations (3, 1.8), (11.4, −1.8) and (7.8, −1.8), respectively. Note that the LECG obtained from the tripolar (figure 6, panel A) and the bipolar (figure 6, panel B) electrodes exhibited similar morphology, polarity and magnitude sequence over the whole area of the chest. Observing figure 6, strong negative waves (area 'a') were shown in both tripolar and bipolar presentations, mainly around the center right side of the sternal midline, namely the subject's left 3rd and 4th rib area. Strong positive waves (area 'b') were discovered in the lower right area, which is actually the subject's left lateral false rib area.

Table 1 presents the SSy of the tripolar and bipolar LECG compared over the central signal in area 'a' in all six subjects. Due to anatomic variations, for each subject the area 'a' which showed strong negative waves over the central chest was located at slightly different positions. Therefore table 1 does not show the SSy at the same location in all six subjects. For example, for subject no 4 (figure 6), SSy(1.8, −1.8) of the tripolar and bipolar LECG were shown in table 1. However, SSy(1.8, 1.8) was described for subject no 3 since that location is where the strong negative signals were seen. A one-tail paired two-sample t-test showed the SSy for the tripolar to be significantly better than for the bipolar LECG ($p = 0.0011$).

Table 1. SSy of the tripolar and bipolar LECG over the area 'a' in all six subjects.

Subject no	SSy(x_0, y_0)	Tripolar	Bipolar
1	SSy(3, 1.8)	1.955	0.963
2	SSy(1.8, 1.8)	2.238	1.153
3	SSy(1.8, 1.8)	3.805	3.318
4	SSy(1.8, −1.8)	3.635	2.371
5	SSy(1.8, 1.8)	2.497	0.651
6	SSy(3, 1.8)	4.334	2.420

Consistent LECG morphology was discovered in all subjects with a few variations in location and magnitude of the waveforms. For example, area 'a' and area 'b' were both present in all six subjects. For subject no 4, area 'a' was located just below the nipple line. However, for subject no 3, area 'a' moved vertically one row upward, which was just above the nipple line. For area 'b', the signals in the 4th row of subject no 1 were much larger than the signals in the 5th row. In figure 6, the same two rows had nearly the same peak-to-peak values. This alteration could result from the effects of the variations in the heart position and conductivities in each subject (Macleod *et al* 2000).

3.3. BSLM

Tripolar BSLM was performed for each subject at the time instant of the Lead II ECG R-wave peak. Multiple localized positive and negative activities are revealed for all six subjects. Figure 7 shows the tripolar BSLM from subject no 4. The physical unit of the color bar/scale in the BSLM is in (mV cm^{-2}). In this map, there are three positive activities denoted by P1, P2 and P3 and two negative activities denoted by N1 and N2.

The pattern characteristics of the BSLM at the instant of the R-wave peak are consistent among all subjects with certain variations in the number of the activities and their locations. The positive activities all occurred in the left inferior chest area and the negative activities appeared over the right anterior central chest. N1 and N2 were present in all six subjects over the central or left central chest with slightly different locations. P3 was seen at nearly the same location in all subjects over the left lateral inferior chest but encompassed slightly different areas. P1 and P2 were both observed in three subjects (nos 2, 4 and 5) with minor location differences. For some subjects whose tripolar BSLM did not exhibit simultaneous P1 and P2 activities, at least one of the activities still occurred, that is, either P1 (subject no 1) or P2 (subjects nos 3 and 6). For subjects no 3 and 6, there is a third negative area shown around the left inferior chest.

3.4. MOA isochronal mapping

The MOA were used to produce isochronal maps of the tripolar LECG on the body surface. The isochrones represent timing of cardiac electrical activation as it reaches the body surface below the active LECG TCE sensors. Figure 8 shows the MOA isochronal map from subject no 4. The propagation time sequence of the cardiac activation as seen on the chest surface with respect to the Lead II ECG R-wave peak is shown using isochrones with the MOA denoted in units of (ms). The range of the MOA was restricted to −40 to 40 ms with isochrones of 5 ms increments shown by bold black lines.

Note that the isochrones of the MOA map, figure 8, had diverse geometric patterns. Regions of sparse (e.g. area with center located at (2, −2)) and crowded (e.g. area with center

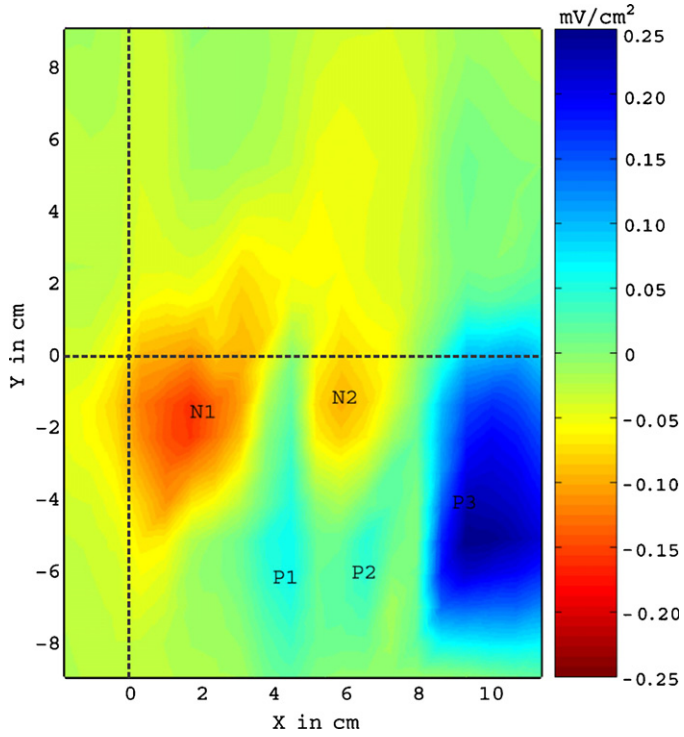

Figure 7. Tripolar BSLM from subject no 4. P1, P2 and P3 denote three positive activities. N1 and N2 denote two negative activities. The abscissa and ordinate (x, y) in (cm) designate the position of the BSLM over the chest. The two dashed lines correspond to the nipple line and sternal midline.

located at (0, 6)) isochrones, indicating spatial nonuniformities of cardiac activation spread, were discovered on the MOA map. The range of MOA in figure 8 is −14.5 ms to 25.5 ms. Multiple localized earlier activation areas were observed. The areas with centers located at (2, −2) and (10, −6) had early MOA isochrones of −10 ms. Other earlier activation time sequences with centers located at (−1.8, 3), (6, −2), (8, −2) and (7, −8) had early MOA isochrones of −5 ms. Positive time sequences showing later activation are viewed over a broad area which is mainly on the top and right side of the map.

For all six subjects the range of MOA is −25 to 31 ms. As the cardiac activation projects to the chest, the earlier activation area over the central or left central chest (e.g. located at (2, −2) in figure 8) is viewed in all six subjects with slightly different locations and occurrence times. The deviation for this earlier area is within a range of 2.5–3.6 cm in X or Y. The variation in the early occurrence time is within 10 ms. For the two earlier activation areas over the left chest (e.g. located at (6, −2) and (8, −2) in figure 8), they were observed simultaneously from two subjects (nos 4 and 6) with slight variation in locations. However for subjects no 1, 2 and 3 only one such earlier area appeared around the left chest. For subject no 5, there is no such earlier area shown. Four subjects (except nos 2 and 6) showed an earlier activation area over the left lateral inferior chest (e.g. located at (10, −6) in figure 8) with minor variation in locations. For the other earlier activation areas among subjects, such as the ones located at (−1.8, 3) in figure 8, there were very large variations which we cannot explain in this study. On the right side of the MOA maps, all six subjects show similar positive timing patterns, delayed activation after the R-wave peak.

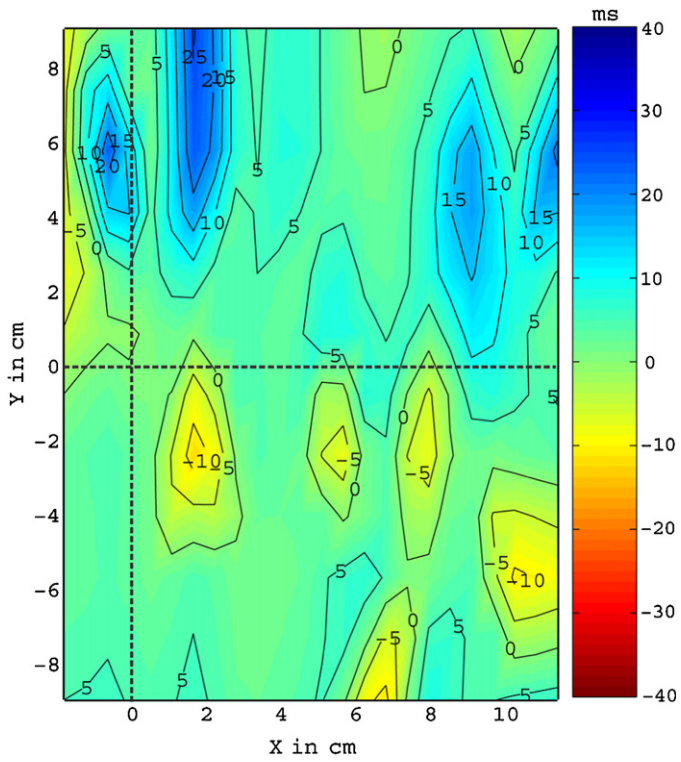

Figure 8. MOA isochronal map showing the timing of the cardiac electrical activation as seen on the chest surface relative to the Lead II ECG R-wave peak for subject no 4. The abscissa and ordinate (x, y) in (cm) designate the position of the MOA map over the chest. The two dashed lines correspond to the nipple line and sternal midline. The redder color/darker shade designates earlier activation with respect to the Lead II ECG R-wave and the bluer color/lighter shade designates the later activation.

4. Discussion

Previous studies (He and Cohen 1991, 1992, 1995, He and Wu 1999, Umetani *et al* 1998, Wu *et al* 1998, 1999, He 1998, Ono *et al* 1997, Lian *et al* 2002a, 2002b, Li *et al* 2002, 2003, He *et al* 2002, Besio and Tarjan 2002a, 2002b, Besio *et al* 2001, Besio 2001, Lu and Tarjan 1999) applied unipolar, bipolar and quasi-bipolar electrodes to record and estimate the LECG. For unipolar electrodes the FPM and spline surface Laplacian estimators were used to derive the LECG from the potential ECG. As a result, it may be sensitive to measurement noise. For the FPM Laplacian estimation, the five discs were shown to be directionally dependent (Geselowitz and Ferrara 1999). Lian *et al* (2001) reported that the directional dependence reported may not be valid. Our new active LECG TCE sensor has a circular symmetrical design, which overcomes the stated directionality problem. Further with the new active LECG TCE sensor, the LECG can be obtained directly from the body surface. This positive aspect could be beneficial when CT and MRI are not available to obtain the body surface geometric parameters that are necessary for the spline LECG estimation (He *et al* 2002, Lian *et al* 2002b, Li *et al* 2003).

Since the skin surface generally conforms to the planar surface of the sensor (Lian *et al* 2001), we can appropriately perform an estimate of the local Laplacian. The dimensions

of the electrode elements on the new active LECG TCE sensor were chosen based on the following three reasons: (a) previous research (Besio *et al* 2001, Besio 2001) used the same electrode element dimensions; (b) the distance between the heart wall and the sensor, which is roughly 3–5 cm, was shown to be the optimal diameter for the outer ring of the concentric ring electrode sensor (Kaufer 1992); (c) the smaller the spacing between the elements, the closer approximation of the 'true' Laplacian, but the weaker the signal. The dimensions chosen assure sufficient amplitude for a reasonable signal-to-noise ratio (SNR).

This paper reports on the experimental investigation of a new active LECG TCE sensor used on a group of six healthy human male subjects. Since the recordings were conducted at 1.2 cm and 3.6 cm intervals in horizontal and vertical directions respectively, the LECG we acquired had higher spatial resolution compared with the other previous LECG recordings (Besio *et al* 2001), 72 versus 35 locations over the same chest area. Another positive attribute is that the inter-element spacing on the new sensor is less than 1.0 cm (figure 1(A)), providing even greater spatial resolution. In this pilot study, the vertical spatial resolution was less than the horizontal resolution. However, in the BSLM and MOA algorithm, vertical and horizontal directions were interpolated to have the same spatial resolution.

In figure 5, the duration of the LECG QRS waves is shorter than that of the Lead II ECG which is consistent with the previous simulation results (He and Cohen 1992) that the LECG has a sharper and narrower shape compared to the ECG. This is why the LECG has a higher spatial resolution than the potential ECG.

Note that the tripolar and bipolar LECG recorded simultaneously using these active LECG TCE sensors show similar activation patterns (figure 6, panels A and B). From both panels in figure 6, we can see the LECG's polarity changes while the cardiac electrical activation is spreading over the whole chest. If the wavefronts are represented by moving dipoles, the dipoles move forward and gyrate as well. The conventional V-leads capture this activity. As the depolarization moves from the right to the left ventricle and downward in the septum and upward in the free wall, the signals go from monophasic negative to monophasic positive and somewhere between the two metamorphose as shown by the biphasic template. The swings may be interpreted as the wavefront moving toward the active LECG TCE sensor exhibiting one direction of polarization, while the departure of the wavefront displays the opposite polarization.

In figure 6 the LECG showed strong signals at a few electrodes around area 'a', whereas most other electrodes far away from area 'a' showed relatively weak signals. Area 'b' also showed strong signals. The signal strength on the body surface depends on many factors including source strength, source orientation and volume conduction properties. For example, the cardiac signals are attenuated due to the low conductivity of the lungs. From the figures, it appears that area 'a' overlaps with the heart base, whereas area 'b' may be near the heart apex.

The SSy, which was calculated at the center of area 'a', was used in this study to directly compare the local sensitivity between the tripolar and bipolar LECG. The SSy for the tripolar LECG in all six subjects is greater than for the bipolar LECG (table 1). This increased SSy may result in tripolar LECG more accurately locating the cardiac activation origins over bipolar LECG. We must clarify that we have not performed invasive experiments to verify where the source is located under our electrode array, but have reported on similar characteristics previously (Besio *et al* 2006).

MOA denotes the activation time on the body surface of the LECG at each recording site and can be used to make isochronal maps. As mentioned previously, the zero-crossing of the LECG (Lu and Tarjan 1999, Kaufer 1992) has been used as a time reference as long as the trajectory of the depolarization wavefront is simple. In such a case zero-crossing occurs when

the vector passes the axis of the sensor (Kaufer 1992). This appears to be an inappropriate model in the present study for at least two reasons: (i) the LECG are not always biphasic waveform (doublet) and (ii) the dipoles move along complicated paths. A new approach with high noise immunity was found when the Lead II ECG was used as a reference and correlated with the LECG (Besio *et al* 2001, Besio 2001, Besio and Kota 2004). The correlation results in leading or lagging times as MOA of the LECG.

Comparing our tripolar BSLM with the previous studies of the FPM and spline BSLM (Wu *et al* 1999 , Li *et al* 2003), the detailed spatial patterns are similar (e.g., N1 in the tripolar BSLM corresponds to N2 reported by Li *et al*; N2 in the tripolar BSLM corresponds to N3 reported by Li *et al;* P1, P2 and P3 in the tripolar BSLM correspond to P2 activity and its subcomponents reported by Wu *et al*). In the MOA isochronal map, we can see multiple earlier activation areas. For subject no 4, in figure 8 the earlier activation area which is located at (2,−2) (also area 'a' in figure 6) coincides with the negative activity N1 in figure 7. This earlier activation area may reflect the earliest epicardial breakthrough of the right ventricle during ventricular depolarization (Wyndham *et al* 1979, Li *et al* 2003). N2 activity appeared at almost the same location as the earlier activation area located at (6, −2). According to Wyndham *et al* (1979), this earlier activation area may be related to the subsequent breakthrough occurring in the left ventricular site anteriorly adjacent to the mid-portion of the septum. P2 activity may be related to the earlier activation area located at (7, −8) with larger variance in location. This earlier activation area may reflect the initial depolarization of the left ventricle (Li *et al* 2003). The earlier activation area center at (10, −6) appears to correspond to P3 activity. It may also reflect the initial depolarization of the left ventricle (Li *et al* 2003). P1 activity cannot be related to any earlier activation area in figure 8.

For the other earlier activation areas located at (8, −2) and (−1.8, 3) in figure 8, we cannot find the corresponding positive or negative activities in figure 7. This may result from the following two reasons. First, the MOA isochronal map may provide more spatiotemporal details than the BSLM. For example, the earlier activation area at (8, −2) in figure 8 may be related to another epicardial breakthrough occurring in the left ventricle. Second, the propagation of the wavefront (or dipole) is very complex. It is affected by the anatomical location or orientation of the heart. And the movement of our sensors on the body surface relative to the heart due to respiration may also cause some distortions of the time sequence. This may also explain why P1 activity cannot be related to any earlier activation area in figure 8.

There were slight variations in the number of the activities, activation times and locations in the tripolar BSLM and MOA maps among subjects. This may be due to differences in body conductivity and variation in heart orientation/position within the chest caused by the body position (Macleod *et al* 2000). However within each subject, the patterns of the multiple activations in the tripolar BSLM and MOA map can be related such that the MOA map can be interpreted with respect to the underlying cardiac electrical activations. For example, for every subject N1 activity can always be related to the corresponding earlier activation area over the central or left central chest of the MOA map. P3 activity can be related to the earlier activation area over the left lateral inferior chest for four subjects (except nos 2 and 6). N2 activity can be related to the earlier activation area around the left chest for four subjects (except nos 1 and 5) with minor location differences.

In some cases, the automated procedure for calculating MOA (Besio and Kota 2004) chose an incorrect value. The Lead II ECG QRS wave is about 100 ms in healthy subjects. Some recording sites lead the R-wave peak and some lag behind. In this study the normal range of the MOA was chosen between −40 ms and 40 ms. If the MOA exceeded this range, it was considered incorrect. In these situations, when making MOA isochronal maps, the

incorrect MOA was discarded manually and its neighbor's MOA were used to interpolate the new MOA for this recording site. In this study, there were on average three incorrect MOA values corrected out of 72 for each subject. The incorrect MOA were in the range of −82 to 112 ms in all six subjects. For example, for subject no 4, the three incorrect MOA values were 87 ms, 104 ms and −79 ms.

In this pilot study, the MOA was derived from the LECG which was recorded on the body surface. Therefore MOA isochronal mapping only provides an approximation of the underlying cardiac activation. We explained the MOA isochronal map with respect to the underlying cardiac electrical events by comparing and relating to the BSLM and previous studies (Wyndham *et al* 1979, Li *et al* 2003). The explanation has not been verified with invasive measurements or other localizing modalities. Since only six subjects have been recorded, no statistical conclusion on the MOA time sequence patterns is available and it is difficult to draw any definitive conclusions on the merits of the TCE-based MOA mapping.

5. Summary

The present study is a pilot study investigating the spatiotemporal patterns of the tripolar BSLM and Laplacian MOA isochronal maps from healthy male subjects using the newly designed active LECG TCE sensor. The long-term goal is to provide a practical non-invasive tool for clinicians diagnosing arrhythmias and assessing the efficacy of therapy. We demonstrated that the active LECG TCE sensor provides enhanced spatial information than the bipolar concentric ring electrode which other authors have shown provides increased spatial frequencies over conventional disc electrodes (He and Cohen 1992). The tripolar BSLM showed similar attributes as the spline BSLM (Li *et al* 2003) but without constructing the surface geometry function. By comparing with the BSLM, the Laplacian MOA isochronal maps may be related to the underlying cardiac activations. The results presented for the six healthy subjects studied are promising considering biological variability. Further work is necessary for clinical validation.

Acknowledgments

The authors thank Dr Peter Tarjan for his advice in editing the manuscript, Dr Wei Jiang for her assistance in hardware testing techniques and all of our lab members for their kindness.

References

Besio W 2001 A study of Laplacian surface maps from moments of activation to detect cardiovascular disease *PhD Dissertation* University of Miami

Besio W, Aakula R, Koka K and Dai W 2006 Development of a tri-polar concentric ring electrode for acquiring accurate Laplacian body surface potentials *Ann. Biomed. Eng.* **34** 426–35

Besio W and Chen T 2006 Non-invasive Laplacian electrocardiography and moment of activation mapping *Proc. 28th Annual Int. Conf. IEEE EMBS*

Besio W and Kota A 2004 Laplacian ECG moment of activation detection algorithm during pacing *Proc. IEEE EMBC* **vol 1** pp 948–51

Besio W, Lu C and Tarjan P 2001 A feasibility study for body surface cardiac propagation maps of humans from Laplacian moments of activation *Electromagnetics* **21** 621–32

Besio W and Tarjan P 2002a Atrial activation pattern from surface Laplacian electrocardiograms of humans *Int. J. Bioelectromagnetism* **4** 95–6

Besio W and Tarjan P 2002b Filtering of surface Laplacian electrocardiograms from humans to produce atrial activation patterns *Proc. IEEE EMBC 2002 and BMES Annual Meeting* pp 1379–80

Fattorusso V and Tilmant J 1949 Exploration du champ electrique precordial a l'aide de deux electrodes circulaires, concentriques et rapprochees *Arch. Mal Coeur* **42** 452–5 (in French)

Geselowitz D B and Ferrara J E 1999 Is accurate recording of the ECG surface Laplacian feasible? *IEEE Trans. Biomed. Eng.* **46** 377–81

He B 1998 Theory and applications of body surface Laplacian ECG mapping *Proc. IEEE EMBC* **17** 102–9

He B and Cohen R 1991 Body surface Laplacian mapping in man *Proc. IEEE EMBC* **13** 784–6

He B and Cohen R 1992 Body surface Laplacian ECG mapping *IEEE Trans. Biomed. Eng.* **39** 1179–91

He B and Cohen R 1995 Body surface Laplacian electrocardiographic mapping—a review *Crit. Rev. Biomed. Eng.* **23** 475–510

He B, Li G and Lian J 2002 A spline Laplacian ECG estimator in a realistic geometry volume conductor *IEEE Trans. Biomed. Eng.* **49** 110–7

He B and Wu D 1997 A bioelectric inverse imaging technique based on surface Laplacians *IEEE Trans. Biomed. Eng.* **44** 529–38

He B and Wu D 1999 Laplacian electrocardiography *Crit. Rev. Biomed. Eng.* **27** 285–338

Kaufer M 1992 Multi-ring sensing electrodes for arrhythmia detection and classification *MS Thesis* University of Miami

Li G, Lian J and He B 2002 On the spatial resolution of body surface potential and Laplacian pace mapping *Pacing Clin. Electrophysiol.* **25** 420–9

Li G, Lian J, Salla P, Cheng J, Shah P, Ramachandra I, Avitall B and He B 2003 Body surface Laplacian ECG mapping of ventricular depolarization in normal subjects *J. Cardiovasc. Electrophysiol.* **14** 6–27

Lian J, Li G, Cheng J, Avitall B and He B 2002b Body surface Laplacian ECG mapping of atrial activation in normal subjects *Med. Biol. Eng. Comput.* **40** 650–9

Lian J, Srinivasan S, Tsai H and He B 2001 Comments on 'Is accurate recording of the ECG surface Laplacian feasible?' *IEEE Trans. Biomed. Eng.* **48** 610–3

Lian J, Srinivasan S, Tsai H, Wu D, Avitall B and He B 2002a On the estimation of noise level and signal to noise ratio of Laplacian ECG during ventricular depolarization and repolarization *Pacing Clin. Electrophysiol.* **25** 1474–87

Lu C and Tarjan P 1999 An ultra-high common-mode rejection ratio (CMRR) AC instrumentation amplifier for Laplacian electrocardiographic measurement *Biomed. Instrum. Technol.* **33** 76–83

Macleod R, Ni Q, Punske B, Ershler P, Yilmaz B and Taccardi B 2000 Effects of heart position on the body surface ECG *Int. Soc. for Computerized Electrocardiography Conference (Yosemite, CA)*

Ono K, Hosaka H and He B 1997 A comparison of body surface Laplacian and potential maps during paced ventricular activation *Methods Info. Med.* **36** 336–8

Oostendorp T F and Oosterom A V 1996 The surface Laplacian of the potential: theory and application *IEEE Trans. Biomed. Eng.* **43** 394–405

Umetani K, Okamoto Y, Mashima S, Ono K, Hosaka H and He B 1998 Body surface Laplacian mapping in patients with left or right ventricular bundle branch block *Pacing Clin. Electrophysiol.* **21** 2043–54

Wu D, Schablowski M, Hosaka H and He B 1998 A simulation study of Laplacian ECG in a realistically shaped torso volume conductor: myocardial infarction *Bioelectrochem. Bioenerg.* **47** 231–5

Wu D, Tsai H and He B 1999 On the estimation of the Laplacian electrocardiogram during ventricular activation *Ann. Biomed. Eng.* **27** 731–45

Wyndham C R, Meeran M K, Smith T, Saxena A, Engelman R M, Levitsky S and Rosen K M 1979 Epicardial activation of the intact human heart without conduction defect *Circulation* **59** 161–8